

Effect of Wave Attenuation on Shear Wave Velocity Determination Using Bender Element Tests

Yanbin Gao ¹, Xiaojun Zheng ¹, Hao Wang ^{2,*} and Wenkang Luo ¹

¹ Department of Geotechnical Engineering, Tongji University, Shanghai 200092, China; yanbin_gao@tongji.edu.cn (Y.G.); 1932639@tongji.edu.cn (X.Z.); 2032242@tongji.edu.cn (W.L.)

² Institute of Acoustics, Tongji University, Shanghai 200092, China

* Correspondence: wanghao@tongji.edu.cn

Abstract: Wave attenuation is a widespread physical phenomenon in most acoustic tests, but there is a scarcity of quantitative investigations into the influence of wave attenuation on the determination of shear wave travel time in bender element tests. To ascertain this attenuation effect, a series of bender element tests were conducted on clay samples with different lengths under unconfined conditions. The experimental results suggest that the real first peak of the received signal attenuates gradually with the increase of the sample length and even becomes undistinguished when the sample length exceeds a limit. This phenomenon results in misinterpretation of the wave travel time using the time domain method. In this study, the shear wave travel time is misinterpreted when wave travel distance over approximately 80 mm, leading to underestimation of the V_S by 17% for the peak-to-peak approach and 10% for the arrival-to-arrival method. Therefore, besides the near field effect and boundary reflection, the wave attenuation effect turned out to be an important factor influencing the determination of V_S using the time domain method. Accordingly, it is advisable to predetermine the limit test distance for a specific testing system under conditions, particularly for long distance testing.

Keywords: bender elements; signal interpretation; wave attenuation; shear wave; time domain method



Citation: Gao, Y.; Zheng, X.; Wang, H.; Luo, W. Effect of Wave Attenuation on Shear Wave Velocity Determination Using Bender Element Tests. *Sensors* **2022**, *22*, 1263. <https://doi.org/10.3390/s22031263>

Academic Editors: Jaroslaw Rybak, Marian Drusa and Andrea Segalini

Received: 31 December 2021

Accepted: 5 February 2022

Published: 7 February 2022

Publisher's Note: MDPI stays neutral with regard to jurisdictional claims in published maps and institutional affiliations.



Copyright: © 2022 by the authors. Licensee MDPI, Basel, Switzerland. This article is an open access article distributed under the terms and conditions of the Creative Commons Attribution (CC BY) license (<https://creativecommons.org/licenses/by/4.0/>).

1. Introduction

The shear wave velocity (V_S) is a fundamental soil parameter, which can be used for liquefaction evaluation [1,2], sample quality assessment [3], and small-strain shear stiffness determination [4]. Since the bender element method was first introduced for soil testing by Shirley and Hampton [5] and Shirley [6], it has been widely installed in geotechnical testing devices to obtain V_S of geotechnical materials (such as clay and sand), including oedometers, direct shear apparatuses, triaxial apparatuses, resonant columns, and even applied in scaled physical model tests. Bender element test commonly adopts transmitter–receiver measurement mode (not the resonant mode) based on the direct-arrive wave principle. The determination of V_S can be expressed as

$$V_S = \frac{L_{tt}}{t} \quad (1)$$

where L_{tt} is the test distance or the travel distance of shear wave (S-wave), i.e., the tip-to-tip length between the bender elements of the transmitter–receiver; and t is the travel time of S-wave. Figure 1a shows the time domain method to determinate the travel time t from the transmitting and received signals, which includes the arrival-to-arrival approach and peak-to-peak approach. In fact, the bender element acts as a finite-length line source, the wave field in bender element test is complex, neither an ideal spherical wave, nor an ideal flat wave. Bender elements generate two P-wave side lobes normal to their plane one in compression and the other in rarefaction, and an S-wave frontal lobe as shown in Figure 1c. The P-wave distortion usually resulting in a reverse deflection before the arrival

of the true S-wave (see Figure 1b). Thus, the initial arrival point of the S-wave is difficult to distinguish and the visual inspected first peak of the S-wave (marked by point A in Figure 1b) is also arguable [7–13]. This distortion is referred to as ‘near field effect’ and it tends to appear when test distance L_{tt} falls in the range of 0.25 to 4 wavelengths (λ) of the received wave [14,15]. In this case, it is widely accepted that point I_3 (zero after the first bump) shown in Figure 1b approximately denotes the arrival of the S-wave [7,15,16]. The near field effect can be effectively eliminated by increase the ratio of L_{tt}/λ , i.e., increasing the excitation frequency or the sample length [14–23]. However, for long soil sample testing, P-wave reflection from the lateral boundary of the soil sample is another potential influencing factor. It can also result in the distortion of the received signals similar with that as shown in Figure 1b. In this case, there is no reliable approach to distinguish the arrival of S-wave from the distorted received signals [24,25]. In order to avoid this kind of distortion, the ratio of length (L) to diameter (D) of the soil sample must be properly considered. Because of these complexities, no standard method has been developed to date for testing and interpretation of the test results. Hence, the results obtained from bender/extender tests are highly subjective in nature and involves high degree of uncertainty [15].

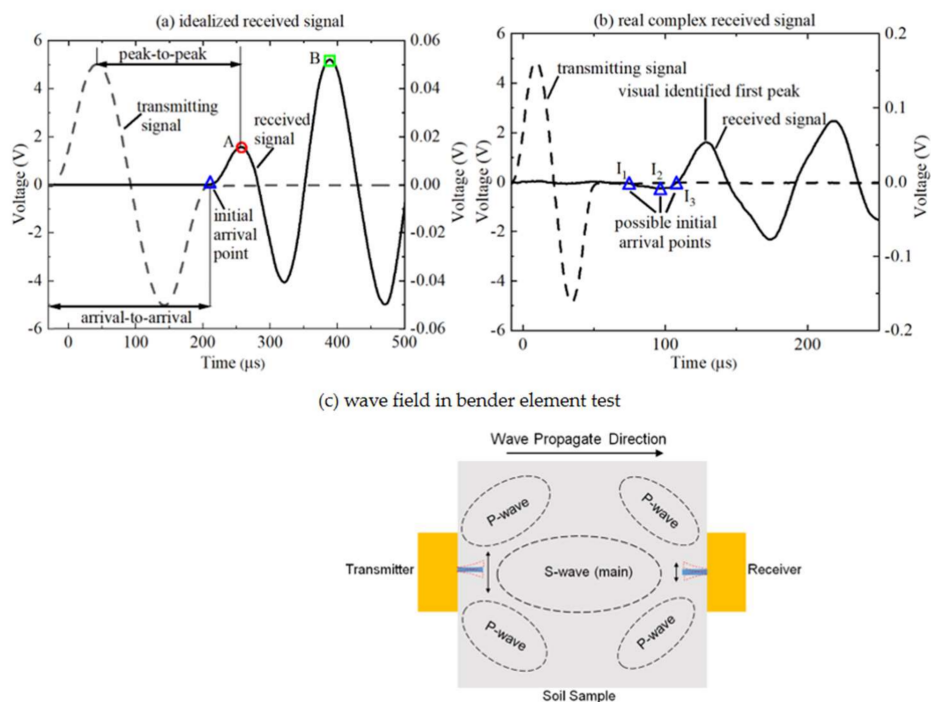


Figure 1. Time domain methods illustrated by (a) idealized received waveform, (b) real complex received waveform, and (c) wave field in bender element test.

Wave attenuation is a basic physical phenomenon in most acoustic tests including bender element tests. Wave attenuation is known to be strongly related to the wave travel distance and the properties of frequency. Table 1 shows some bender element testing conducted on long soil samples or long test distance in the model box. However, literature review shows that the influence of wave attenuation on the received signals and the determination of the travel time of S-wave were rarely investigated in bender element testing. Is the wave attenuation possibly one of the sources of the uncertainty of the interpretation of the test results in bender element test? By comparing the received waveforms of three clay samples with different lengths, Brignoli et al. (1996) reported that the first peak of the received signal tends to attenuate more rapidly than the remaining part of the receiving signal as the test distance increases [26]. Therefore, when the first peak (denoted by A in Figure 1a) attenuates to an imperceptible extent, a risk will be posed because the second peak (denoted by B in Figure 1a) can easily be mistaken for the first peak. In this case, the corresponding results of calculated travel time t and S-wave velocity

V_S will be incorrect. The purpose of this study is thus to delve into the effects of wave attenuation on the determination of S-wave travel time t and the S-wave velocity V_S in the context of the time domain method under long test distance conditions. The scope of tests conducted will be limited in partially saturated clay samples with various lengths.

Table 1. Sample length and test devices/conditions in some selected studies.

References	Test Devices/Conditions	Material	Sample Dimensions or Test Distance (mm)	
			Length (L)	Diameter (D)
[26]	Triaxial test	Consolidated clay	22–95.8	≈ 50
[20]	Model box	Toyoura sand	60–160	/
[27]	Oedometer test	Gault clay	70–150	90
[28]	Resonant column test	Toyoura sand	100	50
[11]	Unconfined	Soft clays mixed with ordinary Portland cement	100	50
[29]	Confined by tube	Dry sand	120–320	50
[30]	Triaxial test	Residual soil from Porto granite	140	70
[9]	Triaxial test	Clay	150	75
[18]	Triaxial test	Fibrous peat organic soil	154	72

2. Materials and Experimental Layout

2.1. Sample Preparation

The reconstructed silty clay was used in this study. The reason why clay is used is that it is difficult to prepare uniform sand samples with different lengths under un-confined conditions. The clay has the following Atterberg limits: plastic limit $PL = 15\%$ and liquid limit $LL = 31\%$. The soil was first air-dried, then the soil blocks were ground and passed through a sieve to prepare the soil powder. The soil powder and water were then mixed in proportions to form a slurry. Next, the slurry was poured into a PVC tube of 60 mm in diameter and 200 mm in length, followed by a one-dimensional consolidation for 72 h under the pressure of 200 kPa. After consolidation, the soil was pushed out from the tube and maintained at room temperature for 24 h to further reduce the moisture content to about 20% and the saturation degree to 60%. Finally, a long cylindrical clay sample was trimmed out with the diameter D of 60 mm and the length L of 125 mm. This long sample was regarded as homogeneous.

2.2. Test Arrangement and Test Procedure

A pair of parallel type bender element sensors were used in this study and the structure of the sensors are shown in Figure 2. The bender element is composed of two piezoelectric bimorphs with external conducting surface, which is installed together with conductive metal in the center. Bender elements were waterproofed by an epoxy coating. The epoxy-coated bender elements are approximately 15 mm squared and 2 mm thick. It was inserted into the sensor shell. The remaining space between the shell and the bender element is filled with silicone rubber. The protruded length of bender element is 2.5 mm. The details of the connection and working principle are also shown in Figure 2. When the input voltage is applied to the transmitter, one piezoelectric sheet extends and the other contracts so that the protruded part moves in thickness direction which generates shear waves in front of the sensor and longitudinal waves on both sides, as shown in Figure 1b. In receive mode, the bender element converts the vibration into an electrical signal output. The resonant frequency of the sensor in air is determined around 3 kHz by the following method mentioned in [25]. The sensor is excited in air with an impact and corroborated by laterally pushing the bender element with a 0.5 mm lead until the lead breaks in bending to simulate a negative step excitation. Then the resonant frequency was calculated from the signal of this free vibration.

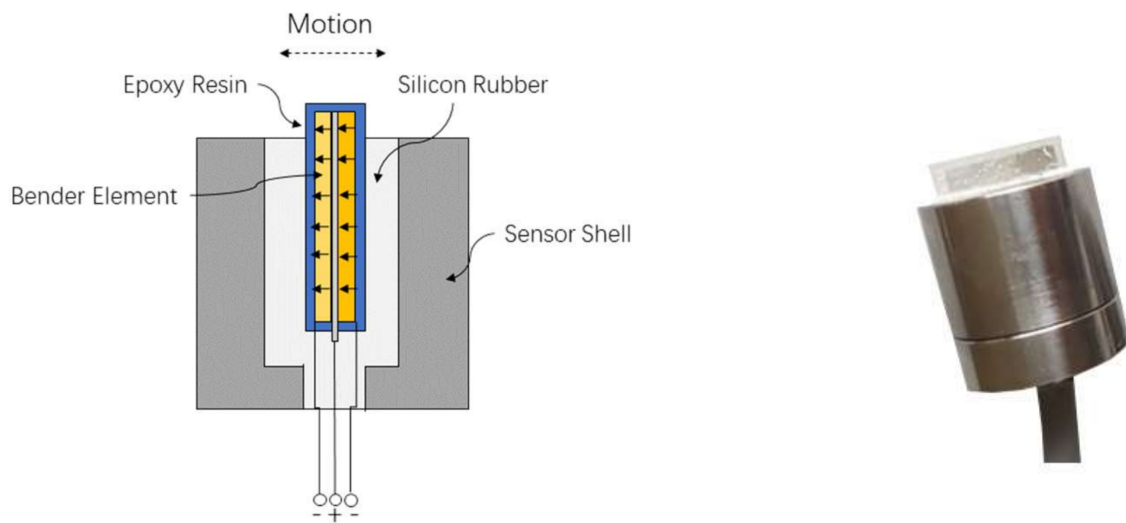


Figure 2. Bender element sensors and its working principle.

The arrangement of the bender element test is shown in Figure 3. For convenience, a sample bracket was used to fix the transmitter and receiver. The sample was fixed between the two bender elements under the unconfined conditions. The protruded part (length 2.5 mm) of the bender elements were directly inserted into the soil sample without couplant. The wave travel distance L_{tt} is the tip-to-tip length of the bender elements, which is 5 mm smaller than the sample length (L). A single cycle sinusoidal signal generated by the function generator is used as the transmitting signal. The voltage amplitude of the transmitting signal is 5 V. By changing the frequency of excitation electrical signal, the frequency of the sinusoidal transmitting signal could vary from 1 to 100 kHz. The electric signal is then converted into a shear wave propagating through the soil sample by the transmitter. Upon being received by the receiver, the shear wave movement is converted into electrical signals, which are amplified by the signal amplifier and captured by a 12-bit high-speed data acquisition board. The maximum digital storage sampling rate is 60×10^6 samples per second. To improve the signal-to-noise ratio, a stacking number of 16 is used. The system delay had been calibrated to be 5 μ s with the bender element tips of the transmitter and receivers in direct contact. The wave propagating through the sample bracket was calibrated to be negligible by comparing the received signals obtained under the conditions of with and without the sample bracket. In bender element testing, excitation frequencies should be properly selected in order to obtain satisfactory signals and best test results. The resonant frequency of the sensors in testing is very different from that determined in air and it is strongly influenced the properties of the soil samples [15]. In bender element test, higher excitation frequencies have the advantages of reducing the near field effect, but it may result in larger wave attenuation. Therefore, different excitation frequency is usually used in bender element test for the best test result. In the literature, the excitation frequency is mostly in the range of 2 kHz to 50 kHz [15]. In this test, input frequencies f selected were 5, 10, 20, and 30 kHz.

The testing process can be summarized as follows. First, the 125 mm length sample was tested. The sample was then trimmed 10 mm off and tested using the four frequencies mentioned above. This test procedure was repeated until the final sample length is 15 mm. Therefore, the number of the tested samples is 12 in total and the L/D varies from 0.25 to 2.08. After the bender element testing, the water content of each trimmed soil was measured and the corresponding values ranged from 18.45% to 18.68%. Due to the slight variation in moisture content, the sample may be considered homogeneous.

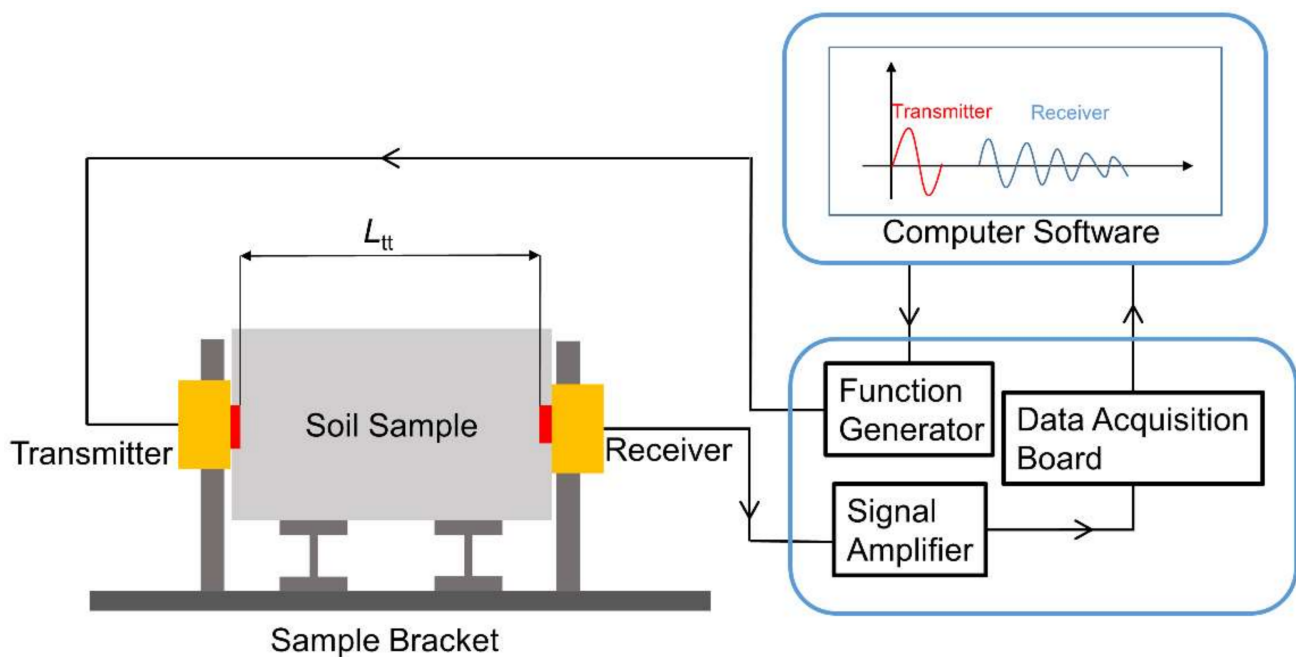


Figure 3. Arrangement of the bender element test.

3. Test Results

3.1. Travel Time Δt and S-Wave Velocity V_S

The received waveforms of the twelve samples measured at $f = 5$ kHz are shown in Figure 4. At this test frequency, the wave number L_{tt}/λ are in the range of 0.28 to 3.33, in which λ is wave length ($\lambda = V_S/f$). These waveforms depict the characteristic points including the initial arrival point (triangle), visually-identified first peaks (upward arrow), real first peaks (point A, circle) and real second peaks (point B, rectangular). The initial arrival point is determined by the zero amplitude after the first bump on received waves (i.e., the I_3 point in Figure 1b) as proposed by [16,31]. It can be seen that there is a marked tendency for point A to attenuate gradually with the increase of L_{tt} . Point A can be easily identified for $L_{tt} \leq 50$ mm ($L_{tt}/\lambda \leq 2.22$), increasingly difficult to identify for $L_{tt} = 60, 70$, and 80 mm and fail to identify for $L_{tt} > 80$ mm. When $L_{tt} > 80$ mm, the visually-identified first peaks are in fact the second peaks, not the real first peaks.

The Δt and V_S were determined by the peak-to-peak approach using the visually-identified first peaks and the arrival-to-arrival approach using the visually-identified initial arrival points (i.e., I_3 point) respectively. The results are shown in Figure 5a,b respectively. For $L_{tt} \leq 80$ mm, the two aforementioned approaches afford practically identical Δt and V_S except for the case of $L_{tt} = 20$ mm, where strong near field effect with a clear traverse waveform emerges before the S-wave arrival (see Figure 4). The V_S is distributed within a limited extent with its average value of 180 m/s. The travel time lines corresponding to $V_S = 180$ m/s are extended to evaluate real initial arrival points and real first peaks for $L_{tt} > 80$ mm and they are shown in Figures 4 and 5a with blue triangle and red circle respectively. Clearly, for $L_{tt} > 80$ mm, the two approaches tend to overestimate Δt and underestimate V_S . Assuming the real $V_S = 180$ m/s, the average relative errors ($= (\text{measured } V_S - \text{real } V_S) / \text{real } V_S \times 100\%$) are approximately -17% and -10% for the peak-to-peak approach and arrival-to-arrival approach, respectively. In this study, arrival-to-arrival approach seems better than the peak-to-peak approach when the first peak cannot be correctly distinguished.

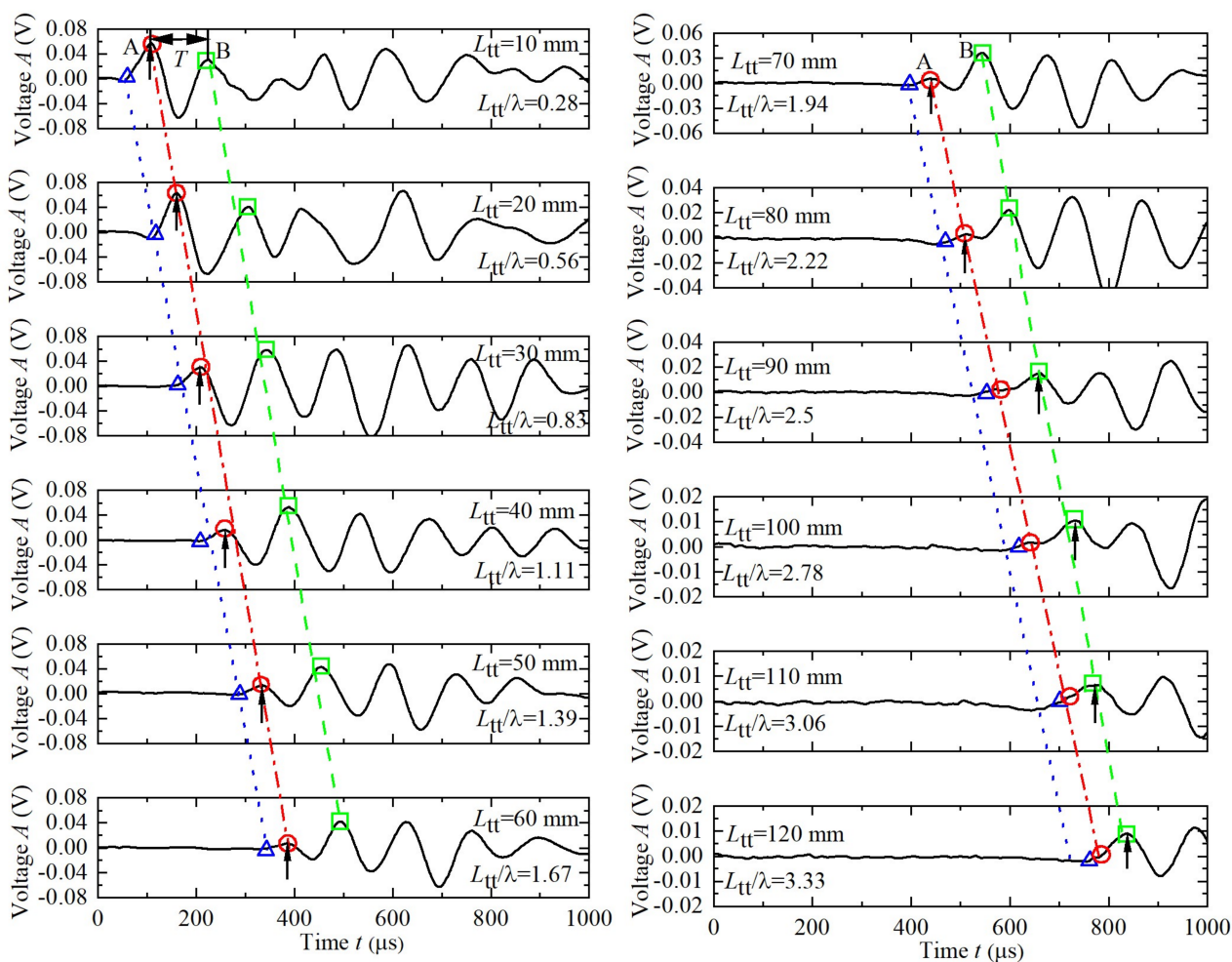


Figure 4. The 12 received waveforms at $f = 5$ kHz.

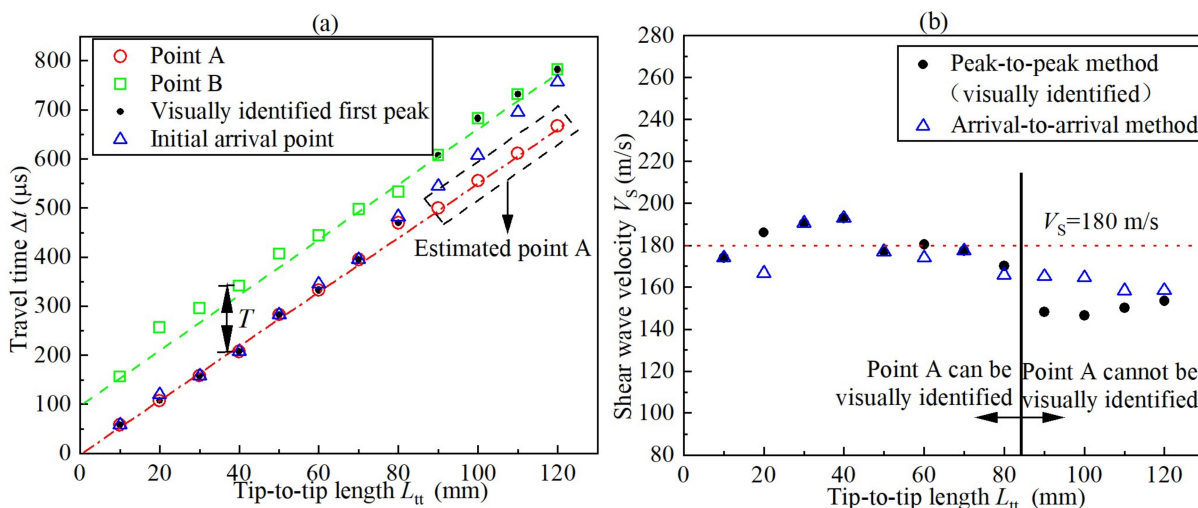


Figure 5. Results of (a) travel time Δt and (b) S-wave velocity V_S ($f = 5$ kHz).

In order to investigate the influence of the test frequency on the test results, Figure 6 describes the received waveforms and the V_S determined for $L_{tt} = 90$ and 120 mm at preceding four frequencies of 5, 10, 20, 30 kHz. In Figure 6, the V_{S1} is the V_S determined by peak-to-peak approach and the V_{S2} is the V_S determined by arrival-to-arrival approach. For $L_{tt} = 90$ mm, although the real first peak was not excited when $f = 5$ kHz, it was excited when $f \geq 10$ kHz ($L_{tt}/\lambda \geq 5$) and the measured V_{S1} and V_{S2} approach $V_S = 180$ m/s.

Nonetheless, for $L_{tt} = 120$ mm, the real first peak was not excited under the four test frequencies and the measured V_{S1} and V_{S2} are approximately 155 m/s. The f_{out} shown in Figure 6 is the excited resonant frequency of the bender element-soil system, which was estimated with the period T of the received signals (see Figure 6) by $f_{out} = 1/T$. When test frequencies were over 10 kHz, the f_{out} approximately stabilized at 12 kHz for $L_{tt} = 90$ mm and 9 kHz for $L_{tt} = 120$ mm, which are larger than the resonant frequency 3 kHz obtained in air without soil sample. These results show that under the test frequency of $f = 10$ kHz which is close to the f_{out} , the real first peak is excited when $L_{tt} = 90$ mm but not when $L_{tt} = 120$ mm. Therefore, the signal enhancement using a resonant test frequency (f approaching f_{out}) proposed by some researchers [25,31,32] is efficient only within a certain test distance in this study.

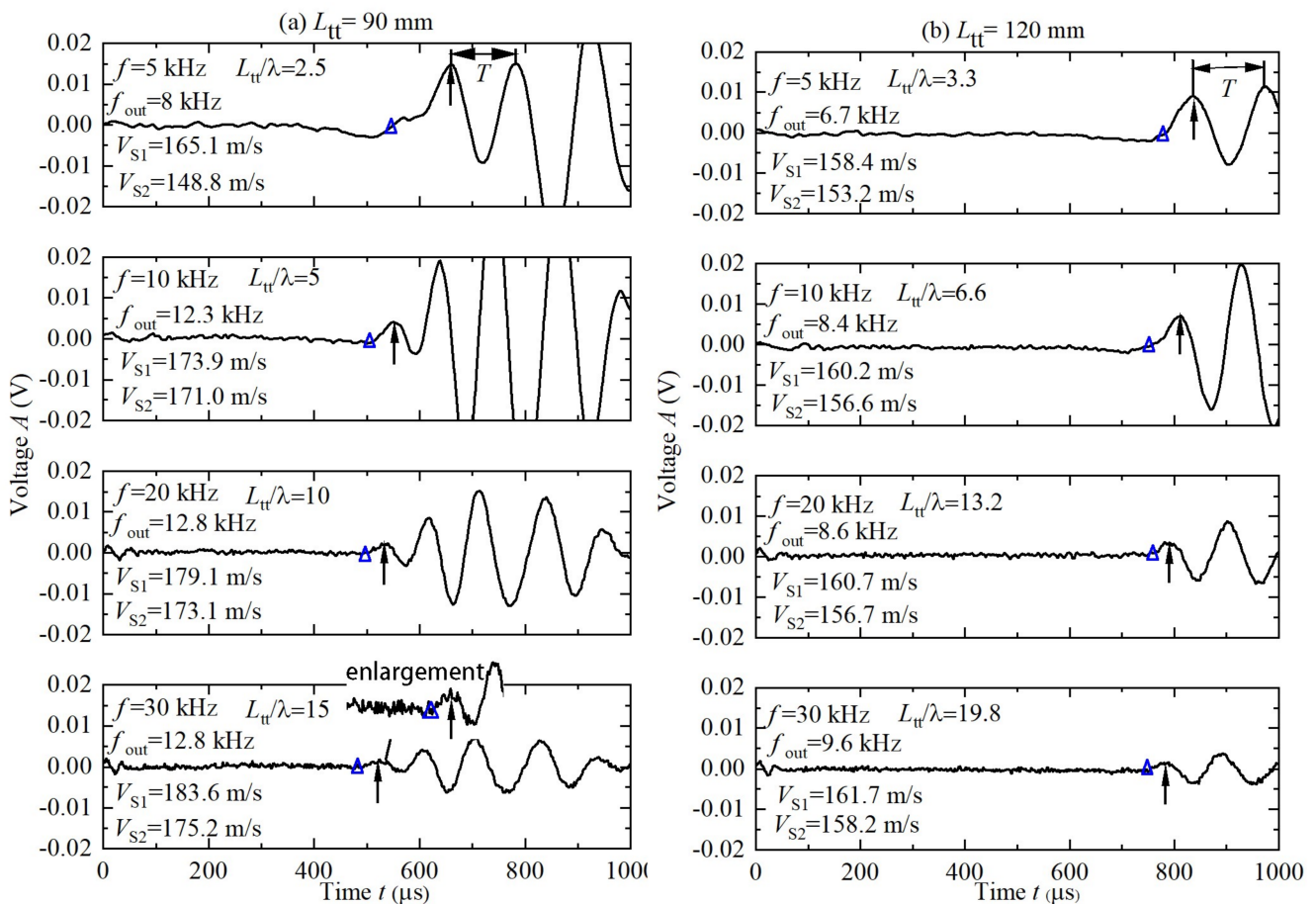


Figure 6. Received waveforms at four testing frequencies: (a) $L_{tt} = 90$ mm; (b) $L_{tt} = 120$ mm.

3.2. Attenuation of Peak Points

Figure 7 shows the relationships of the received voltage amplitude (A_m) of the real first peak A against the test length L_{tt} at the four frequencies in two kinds of scales. It can be seen that A_m of real first peak A decreased significantly with the increase of L_{tt} . The received voltage amplitude (A_m) of the real first peak A is entirely below 0.08 V, which is considerably much smaller than the input voltage amplitude 5 V. This significant attenuation mainly arises from the factors including transformation between voltage and mechanical wave, bender element-soil interactions, sample absorption, and dispersion in surrounding air/materials. The critical value for the identification of first peak is approximately 0.002 V. The linear $\ln(A_m)$ versus L_{tt} relationships shown in Figure 7b indicate the attenuation following the exponential relationship. A decreasing trend in A_m with test frequencies f is observed, except for $f = 10$ kHz which approaching the resonant frequency f_{out} .

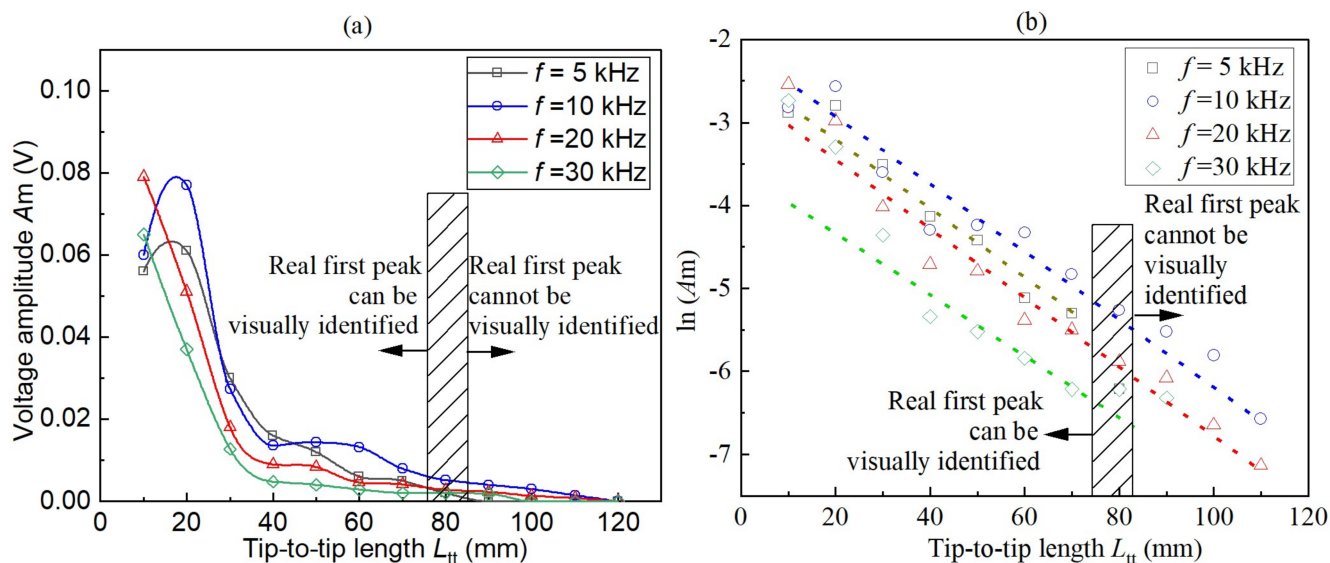


Figure 7. Attenuation curves of real first peak A in (a) A_m - L_{tt} scale and (b) $\ln(A_m)$ - L_{tt} scale.

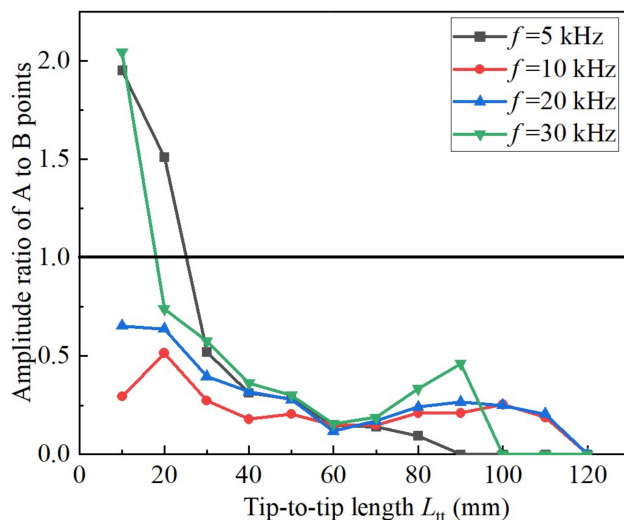


Figure 8. Amplitude ratio of peak point A to peak point B.

Figure 8 shows the amplitude ratio of point A to point B, i.e., real first peak to real second peak. The ratios are primarily smaller than 1.0, indicating the amplitude of point A is smaller than point B. The ratios generally decrease with L_{tt} , indicating that point A attenuates more significantly than point B as L_{tt} increases. This feature is also reported in [26]. It is possibly related to the frequency components of the waveform involved: point A contains higher frequency components, thereby exhibiting more remarkable attenuation. However, this hypothesis needs to be tested with more information.

4. Discussion

According to the test results, Figure 9 summarized the three modes of the received signals related to wave attenuation. Mode A is a normal one, in which the attenuation is not significant and the real first peak of the S-wave can be clearly distinguished. In mode B, wave attenuation makes the real first peak undistinguished, but the revised part of the first cycle can still be distinguished. Under this condition, the received signal is very similar to that given in Figure 1b and the revised signal is very easy to be mistaken as the P-wave distortion in near field effect or boundary reflection. In mode C, the first cycle is completely undistinguished, both peak-to-peak approach and arrival-to-arrival approach may underestimate the V_S significantly. In any case, the wave attenuation may make the

over-estimation of the S-wave travel time and under-estimation of the S-wave velocity. Therefore, it is very different from the P-wave distortion mentioned in the Introduction part in this paper, which will make the over-estimation of the S-wave travel time and under-estimation of the S-wave velocity.

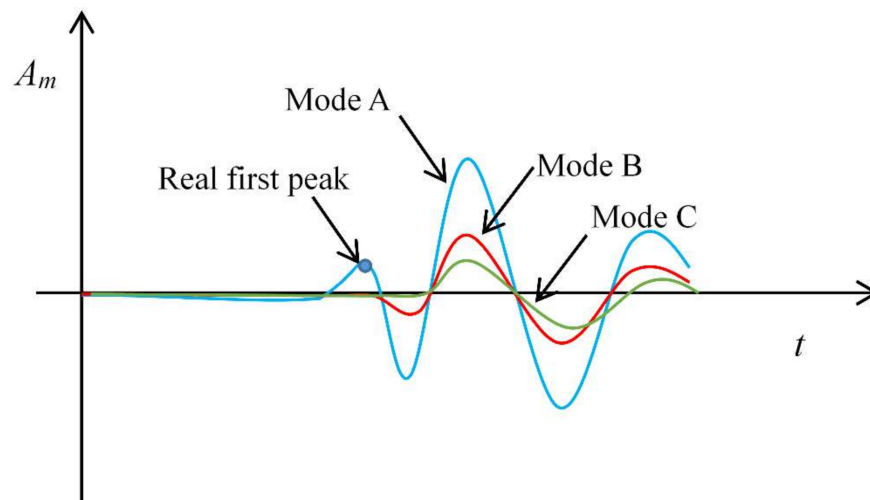


Figure 9. Three modes of received signals related to wave attenuation.

The errors for mode C, arising from the imperceptible first cycle of received waveform, can be estimated using the period T (i.e., time difference between the first peak and second peak) as follows

$$\text{Relative error of } V_s = \frac{\text{measured } V_s - \text{real } V_s}{\text{real } V_s} = \frac{L_{tt}/(\Delta t + T) - L_{tt}/\Delta t}{L_{tt}/\Delta t} = -\frac{T}{\Delta t + T} (\times 100\%) \quad (2)$$

in which Δt is real travel time and $\Delta t + T$ is visually-identified travel time with an error of T because of attenuation. According to Figure 5a, the period T maintains almost constant at $100 \mu\text{s}$ under $f = 5 \text{ kHz}$ for various L_{tt} . According to Equation (2), because Δt increases with L_{tt} , the relative error will decrease with L_{tt} . It agrees well with results of peak-to-peak approach given in Figure 5b. The deviation of arrival-to-arrival approach from Equation (1) is presumably attributed to the complexity of waveform around the S-wave arrival: a slight reverse occurs before the arrival of S-wave when $L_{tt} \geq 80 \text{ mm}$ (see Figure 4). This slight reverse is possibly resulting from the light boundary reflection of P wave under long test distance [24,33].

Ingale et al. (2017) summarized the factors influencing the wave attenuation in bender element tests [15]. The absorbing attenuation is closely associated with the damping characteristics of soil which is determined by soil type, moisture content, and stress state [17,34,35]. The influence of testing confining pressure on the received waveform has been studied with contrary conclusions. For example, the results of [36] using fully saturated kaolin in ultrasonic testing show that wave attenuation can be reduced with an increase of confining pressure. Conversely, other researchers observed that the amplitude of the received waveform decreases with increasing confining pressure in their bender element tests using dry sand [33,37]. Arguably, the consolidation process and confining pressure may be beneficial to lessen the wave attenuation effect merely for clay samples. Adopting higher length-to-thickness ratio to achieve low resonant frequency is also an available method to reduce the wave attenuation [15]. In principle, wave attenuation can also be reduced by improving the performance of testing system. Approaches include: (1) using the digital oscilloscopes with high analog to digital conversion resolution (≥ 12 bits) [21,38], (2) parallel connection and series connection as a transmitter and a receiver, respectively [21], (3) increases the signal to noise ratio of the received waveforms by using a large voltage applied to transmitters [21]. However, theoretically the wave attenuation effect will always matter when L_{tt} exceeds a

critical value, which is concerned with material properties, test equipment, sample characteristics, and test conditions. Consequently, it is advisable to carefully pre-determine the corresponding critical length of the test system using different sample length or test distance, so that the accurate velocity can be obtained.

5. Conclusions

Wave attenuation in bender element testing has been observed here to serve as a contributing factor influencing received waveforms and shear wave velocity determination by the time domain method for long samples. In this study on unsaturated clay samples, the wave arrival time is prone to be misinterpreted for the cases with wave travel distance over approximately 80 mm, thereby leading to underestimation of the V_S by 17% on average for the peak-to-peak approach and 10% and on average for the arrival-to-arrival approach. Three modes of the received signals related to wave attenuation are summarized. In any case, the wave attenuation may make the over-estimation of the S-wave travel time and under-estimation of the V_S . This effect is fundamentally different from the P-wave distortion, which results in the over-estimation of the S-wave travel time and under-estimation of the V_S . The wave attenuation effect may be minimized with an appropriate excitation frequency or improved testing system. However, given that this effect cannot be totally eliminated in theory, when involving long distance testing with high test frequency, it is suggested that the wave attenuation characteristic and critical test length for a testing system should be calibrated with caution.

Author Contributions: Conceptualization, Y.G.; Methodology, X.Z.; Software, H.W.; Validation, X.Z. and W.L.; Formal analysis, Y.G. and H.W.; Investigation, Y.G.; Resources, H.W.; Data curation, X.Z.; Writing—original draft preparation, X.Z.; Writing—review and editing, Y.G.; Visualization, X.Z.; Supervision, Y.G.; Project administration, Y.G. and H.W.; Funding acquisition, Y.G. All authors have read and agreed to the published version of the manuscript.

Funding: This research was funded by the National Natural Science Foundation of China (Grant No. 41972273, 41772293).

Institutional Review Board Statement: Not applicable.

Informed Consent Statement: Not applicable.

Data Availability Statement: The data presented in this study are available on request from the corresponding author.

Conflicts of Interest: The authors declare no conflict of interest.

References

1. Zhou, T.G.; Chen, T.M. Laboratory investigation on assessing liquefaction resistance of sandy soils by shear wave velocity. *J. Geotech. Geoenviron. Eng.* **2007**, *133*, 959–972. [[CrossRef](#)]
2. Kayen, R.; Moss, R.E.S.; Thompson, E.M.; Seed, R.B.; Cetin, K.O.; Kiureghian, A.D.; Tanaka, Y.; Tokimatsu, K. Shear-wave velocity-based probabilistic and deterministic assessment of seismic soil liquefaction potential. *J. Geotech. Geoenviron. Eng.* **2013**, *139*, 407–419. [[CrossRef](#)]
3. Landon, M.M.; DeGroot, D.J.; Sheahan, T.C. Nondestructive sample quality assessment of a soft clay using shear wave velocity. *J. Geotech. Geoenviron. Eng.* **2007**, *133*, 424–432. [[CrossRef](#)]
4. Richart, F.E.; Hall, J.R.; Woods, R.D. *Vibrations of Soils and Foundations*; Prentice Hall: Englewood Cliffs, NJ, USA, 1970.
5. Shirley, D.J.; Hampton, L.D. Shear-wave measurements in laboratory sediments. *J. Acoust. Soc. Am.* **1978**, *63*, 607–613. [[CrossRef](#)]
6. Shirley, D.J. An improved shear wave transducer. *J. Acoust. Soc. Am.* **1978**, *63*, 1643–1645. [[CrossRef](#)]
7. Viggiani, G.; Atkinson, J. Interpretation of bender element tests. *Géotechnique* **1995**, *45*, 149–154. [[CrossRef](#)]
8. Wang, Y.; Benahmed, N.; Cui, Y.J.; Tang, A.M. A novel method for determining the small-strain shear modulus of soil using the bender elements technique. *Can. Geotech. J.* **2017**, *54*, 280–289. [[CrossRef](#)]
9. Ogino, T.; Kawaguchi, T.; Yamashita, S.; Kawajiri, S. Measurement deviations for shear wave velocity of bender element test using time domain, cross-correlation, and frequency domain approaches. *Soils Found.* **2015**, *55*, 329–342. [[CrossRef](#)]
10. Gu, X.; Yang, J.; Huang, M. Laboratory measurements of small strain properties of dry sands by bender element. *Soils Found.* **2013**, *53*, 735–745. [[CrossRef](#)]

11. Khan, Q.; Moon, S.; Ku, T. Idealized sine wave approach to determine arrival times of shear wave signals using bender elements. *Geotech. Test. J.* **2019**, *43*, 171–193. [[CrossRef](#)]
12. Kumar, J.; Madhusudhan, B.N. A note on the measurement of travel times using bender and extender elements. *Soil Dyn. Earthq. Eng.* **2010**, *30*, 630–634. [[CrossRef](#)]
13. Cai, Y.; Dong, Q.; Wang, J.; Gu, C.; Xu, C. Measurement of small strain shear modulus of clean and natural sands in saturated condition using bender element test. *Soil Dyn. Earthq. Eng.* **2015**, *76*, 100–110. [[CrossRef](#)]
14. Arroyo, M.; Muir Wood, D.; Greening, P. Source near-field effects and pulse tests in soil samples. *Géotechnique* **2003**, *53*, 337–345. [[CrossRef](#)]
15. Ingale, R.; Patel, A.; Mandal, A. Performance analysis of piezoceramic elements in soils: A review. *Sens. Actuator A-Phys.* **2017**, *262*, 46–63. [[CrossRef](#)]
16. Yamashita, S.; Kawaguchi, T.; Nakata, Y.; Mikami, T.; Fujiwara, T.; Shibuya, S. Interpretation of international parallel test on the measurement of G_{\max} using bender elements. *Soils Found.* **2009**, *49*, 631–650. [[CrossRef](#)]
17. Sanchez-Salinero, I.; Roesset, J.M.; Stokoe, I.; Kenneth, H. *Analytical Studies of Body Wave Propagation and Attenuation*; Geotechnical Engineering Report No. GR 86-15; University of Texas: Austin, TX, USA, 1986.
18. Arulnathan, R.; Boulanger, R.W.; Riemer, M.F. Analysis of bender element tests. *Geotech. Test. J.* **1998**, *21*, 120–131.
19. Pennington, D.S.; Nash, D.F.; Lings, M.L. Horizontally mounted bender elements for measuring anisotropic shear moduli in triaxial clay specimens. *Geotech. Test. J.* **2001**, *24*, 133–144.
20. Wang, Y.H.; Lo, K.F.; Yan, W.M.; Dong, X.B. Measurement biases in the bender element test. *J. Geotech. Geoenviron. Eng.* **2007**, *133*, 564–574. [[CrossRef](#)]
21. Leong, E.C.; Yeo, S.H.; Rahardjo, H. Measuring shear wave velocity using bender elements. *Geotech. Test. J.* **2005**, *28*, 488–498.
22. Fam, M.; Santamarina, J.C. Study of geoprocesses with complementary mechanical and electromagnetic wave measurements in an oedometer. *Geotech. Test. J.* **1995**, *18*, 307–314.
23. Gajo, A.; Fedel, A.; Mongiovi, L. Experimental analysis of the effects of fluid-solid coupling on the velocity of elastic waves in saturated porous media. *Géotechnique* **1997**, *47*, 993–1008. [[CrossRef](#)]
24. Arroyo, M.; Muir Wood, D.; Greening, P.; Medina, L.; Rio, J. Effects of sample size on bender-based axial G_0 measurements. *Géotechnique* **2006**, *56*, 39–52. [[CrossRef](#)]
25. Lee, J.S.; Santamarina, J.C. Bender elements: Performance and signal interpretation. *J. Geotech. Geoenviron. Eng.* **2005**, *131*, 1063–1070. [[CrossRef](#)]
26. Brignoli, E.; Gotti, M.; Stokoe, K.H. Measurement of shear waves in laboratory specimens by means of piezoelectric transducers. *Geotech. Test. J.* **1996**, *19*, 384–397.
27. Arroyo, M.; Greening, P.; Muir Wood, D. An estimate of uncertainty in current pulse test practice. *Rivista Italiana di Geotecnica* **2003**, *37*, 17–35.
28. Gu, X.; Yang, J.; Huang, M.; Gao, G. Bender element tests in dry and saturated sand: Signal interpretation and result comparison. *Soils Found.* **2015**, *55*, 951–962. [[CrossRef](#)]
29. Huang, L.; Wang, Y.; Li, J.; He, W.; Li, X. The effect of different boundary conditions on the result of bender-extender element test. In Proceedings of the International Conference on Geotechnical and Earthquake Engineering 2018: Geotechnical and Seismic Research and Practices for Sustainability, IACGE, Chongqing University, Chongqing, China, 20 October 2018.
30. Viana da Fonseca, A.V.; Ferreira, C.; Fahey, M. A framework interpreting bender element tests, combining time-domain and frequency-domain methods. *Geotech. Test. J.* **2009**, *32*, 91–107.
31. Kawaguchi, T.; Mitachi, T.; Shibuya, S. Evaluation of shear wave travel time in laboratory bender element test. In Proceedings of the Fifteenth International Conference on Soil Mechanics and Geotechnical Engineering, Istanbul, Turkey, 27–31 August 2001; pp. 155–158.
32. Jovicic, V.; Coop, M.R.; Simic, M. Objective criteria for determining G_{\max} from bender element tests. *Géotechnique* **1996**, *46*, 357–362. [[CrossRef](#)]
33. Marjanovic, J.; Germaine, J.T. Experimental study investigating the effects of setup conditions on bender element velocity results. *Geotech. Test. J.* **2013**, *36*, 1–11. [[CrossRef](#)]
34. Youn, J.U.; Choo, Y.W.; Kim, D.S. Measurement of small-strain shear modulus G_{\max} of dry and saturated sands by bender element, resonant column, and torsional shear tests. *Can. Geotech. J.* **2008**, *45*, 1426–1438. [[CrossRef](#)]
35. Xu, K.; Gu, X.; Hu, C.; Lu, L. Comparison of small-strain shear modulus and Young's modulus of dry sand measured by resonant column and bender-extender element. *Can. Geotech. J.* **2020**, *57*, 1745–1753. [[CrossRef](#)]
36. Leong, E.C.; Yeo, S.H.; Rahardjo, H. Measurement of wave velocities and attenuation using an ultrasonic test system. *Can. Geotech. J.* **2004**, *41*, 844–860. [[CrossRef](#)]
37. Lings, M.L.; Greening, P.D. A novel bender/extender element for soil testing. *Géotechnique* **2001**, *51*, 713–717. [[CrossRef](#)]
38. Leong, E.C.; Cahyadi, J.; Rahardjo, H. Measuring shear and compression wave velocities of soil using bender-extender elements. *Can. Geotech. J.* **2009**, *46*, 792–812. [[CrossRef](#)]